

Enhancement of Curie temperature in Mn₂RuSn by Co substitution

A. Nelson,¹ P. Kharel,^{1,2,a)} Y. Huh,¹ R. Fuglsby,¹ J. Guenther,¹ W. Zhang,^{2,3} B. Staten,⁴ P. Lukashev,⁴ S. Valloppilly,² and D. J. Sellmyer^{2,3}

¹Department of Physics, South Dakota State University, Brookings, South Dakota 57007, USA

²Nebraska Center for Materials and Nanoscience, University of Nebraska, Lincoln, Nebraska 68588, USA

³Department of Physics and Astronomy, University of Nebraska, Lincoln, Nebraska 68588, USA

⁴Department of Physics, University of Northern Iowa, Cedar Falls, Iowa 50614, USA

(Received 29 January 2015; accepted 9 April 2015; published online 21 April 2015)

The Co-substituted Mn₂RuSn nanomaterials, namely, Mn₂Ru_{0.5}Co_{0.5}Sn and Mn₂Ru_{0.35}Co_{0.65}Sn have been synthesized and investigated. The presence of Co in the Mn₂RuSn ($a = 6.21 \text{ \AA}$) decreased the lattice parameter, where $a = 6.14 \text{ \AA}$ and 6.12 \AA for the as prepared Mn₂Ru_{0.5}Co_{0.5}Sn and Mn₂Ru_{0.35}Co_{0.65}Sn, respectively. The samples show a ferrimagnetic spin order with relatively small coercivities, similar to those of soft magnetic materials. There is a substantial increase in the Curie temperature ($T_c = 448 \text{ K}$ for Mn₂Ru_{0.5}Co_{0.5}Sn and 506 K for Mn₂Ru_{0.35}Co_{0.65}Sn) of Mn₂RuSn ($T_c = 272.1 \text{ K}$) due to Co substitution, which is a result of strengthening of the positive exchange interaction in this material. These materials are highly stable against heat treatment of up to 450°C . The first-principles calculations are consistent with our experimentally observed structural and magnetic properties. They also provide insight on how the magnetic and electronic structures change when Ru is replaced with Co in Mn₂RuSn. © 2015 AIP Publishing LLC.

[<http://dx.doi.org/10.1063/1.4918664>]

I. INTRODUCTION

Mn-based Heusler compounds have attracted significant attention because of their multifunctional properties including half-metallic high temperature ferri- and ferromagnetism,^{1–4} and shape memory effect.^{5,6} Some of the Mn-based alloys including Mn_{3-x}Ga ($x = 2–3$) crystallize in a tetragonal structure with high perpendicular magnetic anisotropy (PMA) and high spin polarization at the Fermi level showing huge potential for the spin transfer torque (STT)-based non-volatile memory and logic devices.^{2,7} An ideal material for STT-based spintronic devices should exhibit high PMA combined with high spin polarization at the Fermi level and low net magnetization, the latter to minimize field effects.² Recently, an interesting materials property, namely, spin gapless semiconductivity has been reported in another Mn-based Heusler compound Mn₂CoAl.⁸ In spin gapless semiconductors, not only electrons but also holes are 100% spin polarized and the spin-polarized electron-conduction can be tuned between p-type and n-type by adjusting the gate voltage, offering a superior device performance as compared to that of half metals and diluted magnetic semiconductors.^{9,10}

One of the main issues with these materials is the site disorder, where two or more atomic species tend to occupy the same set of Wyckoff positions, which is detrimental to half metallicity.^{11,12} In general, the regular Heusler compounds (X₂YZ) crystallize in the cubic L₂₁ structure (prototype-Cu₂MnAl, space group Fm $\bar{3}$ m, No.225), where X, Y, and Z atoms, respectively, occupy the Wyckoff's 8c ($1/4, 1/4, 1/4$), 4b ($1/2, 1/2, 1/2$), and 4a (0,0,0) positions. Some of the Mn-based compounds also crystallize in the

inverse Heusler structure (Prototype-CuHg₂Ti, Space group F43m, No. 216), where X atoms are located at the Wyckoff's 4a (0, 0, 0) and 4d ($3/4, 3/4, 3/4$) positions, while the Y and the Z atoms are located at 4b ($1/2, 1/2, 1/2$) and 4c ($1/4, 1/4, 1/4$) positions, respectively. However, in practice, many of these Heusler compounds crystallize either with partially disordered B2-type (half of the Y and Z atoms interchange their positions, where the 4a and 4b sites become equivalent) or fully disordered A2-type (X, Y, and Z atoms are randomly distributed at all available lattice sites) phase.¹¹ Therefore, it is very important to identify novel Heusler compounds in which the electronic band properties are less sensitive to disorder. Our interest is to investigate one of such compounds Mn₂RuSn, which is predicted to be less sensitive to B2-type disorder.¹³

Mn₂RuSn has been reported to crystallize in the inverse Heusler structure (XA structure).^{13,14} However, experimentally only a disordered phase (L₂₁B) has been synthesized.^{15,16} It has been predicted that this material can show a half-metallic band structure (100% spin polarization) for the lattice parameter a from 5.9 \AA to 6.1 \AA , which is slightly smaller than the experimentally observed value of 6.21 \AA .^{13,16} The experimental values of the saturation magnetization and Curie temperature of bulk Mn₂RuSn are $1.68 \mu_B/\text{f.u.}$ and 272.1 K , respectively.¹⁶ Our goal is to investigate how the structural, magnetic, and electronic band properties of Mn₂RuSn change when a fraction of Ru is replaced with Co atoms of smaller atomic sizes. Here, we present our experimental investigations on Mn₂Ru_{0.5}Co_{0.5}Sn and Mn₂Ru_{0.35}Co_{0.65}Sn nanomaterials and first-principles calculations of Mn₂RuSn and Mn₂Ru_{0.5}Co_{0.5}Sn and show that the Curie temperature of Mn₂RuSn can be substantially increased by replacing a fraction of Ru with Co.

^{a)}parashu.kharel@sdstate.edu

II. EXPERIMENTAL AND COMPUTATIONAL METHODS

The $\text{Mn}_2\text{Ru}_{1-x}\text{Co}_x\text{Sn}$ ($x = 0.5, 0.65$) nanomaterials in the form of ribbons were prepared using arc-melting and melt-spinning. The ribbon samples were synthesized by ejecting induction-melted solutions of $\text{Mn}_2\text{Ru}_{1-x}\text{Co}_x\text{Sn}$ onto the surface of a copper wheel rotating with a speed of 28 m/s in a chamber filled with highly pure argon. In order to investigate the effect of annealing on the crystal structure and magnetic properties, the ribbons were annealed in a tubular furnace pumped to a base pressure of about 10^{-7} Torr at temperatures 250 °C and 450 °C for 2 h. The elemental compositions were confirmed using energy dispersive x-ray spectroscopy (EDX), which showed that the compositions were close to the estimated values within an error of 0.1 at. %. The structural properties of the samples were studied by x-ray diffraction (XRD) using a Rigaku MiniFlex with a copper source. The magnetic properties were investigated with a Quantum Design VersaLab magnetometer and a SQUID magnetometer. The Rietveld analysis of the x-ray diffraction patterns was done using TOPAS software.¹⁷

In order to better interpret the experimental results, we have performed the electronic band-structure calculations of bulk Mn_2RuSn and $\text{Mn}_2\text{Ru}_{0.5}\text{Co}_{0.5}\text{Sn}$ in cubic phase. We have performed density-functional calculations using the projector augmented wave method (PAW) by Blöchl,¹⁸ implemented by Kresse and Joubert in the Vienna *ab initio* simulation package (VASP)¹⁹ within the Perdew-Burke-Ernzerhof (PBE) generalized gradient approximation (GGA).²⁰ The Methfessel-Paxton integration method²¹ with a 0.05 eV width of smearing is used, along with a plane-wave cut-off energy of 500 eV and convergence criteria of 10^{-3} meV for the total energy

calculations. A $12 \times 12 \times 12$ k-points mesh is used for the Brillouin zone integration.

III. EXPERIMENTAL RESULTS

A. Structural properties

The room-temperature XRD patterns of the $\text{Mn}_2\text{Ru}_{0.5}\text{Co}_{0.5}\text{Sn}$ and $\text{Mn}_2\text{Ru}_{0.35}\text{Co}_{0.65}\text{Sn}$ ribbons are shown in Figs. 1(a) and 1(b), respectively. These figures also include the patterns from corresponding samples annealed in vacuum furnace at 250 °C and 450 °C. Almost all intense peaks in the XRD patterns are indexed with the reported standard patterns for Mn_2RuSn alloy in the cubic $L2_1\text{B}$ -type crystal structure.¹⁶

In order to further understand the crystal structure and alloy phases, we have carried out the Rietveld analysis of the XRD patterns using TOPAS software. Initially, we compared simulated powder diffraction patterns based on structure models of $L2_1\text{A}$, XA , and $L2_1\text{B}$ -types of atomic ordering with the experimental diffraction pattern. A clear distinction between these structures is only possible based on the analysis of very weak Bragg reflections such as (111), (200), (222) and (420), making the process extremely difficult. However, our preliminary analysis suggested that the structure may be more towards the $L2_1\text{B}$ type and we have therefore used this as the starting model for refinement. The powder diffraction patterns were simulated and refined with $(\text{Mn}_{0.5}\text{Ru}_{1-x}\text{Co}_x)_2$ randomly occupying the 4a (0, 0, 0) and 4b (1/2, 1/2, 1/2) positions and Mn and Sn occupying the 4d (3/4, 3/4, 3/4) and Sn at 4c (1/4, 1/4, 1/4) positions, respectively. The refinement also suggested minor site sharing of Ru with Mn at 4d site for $x = 0.65$ case. Further, some minor (001) texture was also included in the refinement to obtain the best agreement.

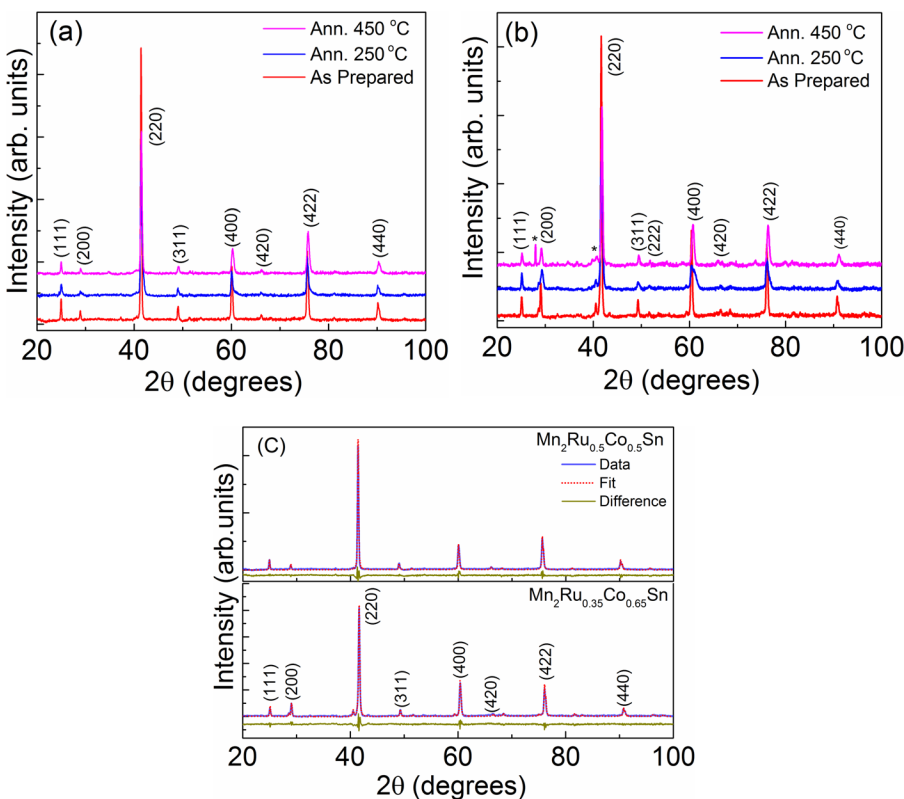


FIG. 1. Room-temperature x-ray diffraction patterns of (a) $\text{Mn}_2\text{Ru}_{0.5}\text{Co}_{0.5}\text{Sn}$ and (b) $\text{Mn}_2\text{Ru}_{0.35}\text{Co}_{0.65}\text{Sn}$ ribbons. In both the figures, the patterns of as-prepared, 250 °C-annealed and 450 °C-annealed samples are arranged from bottom to top, respectively. (c) The simulated powder diffraction patterns for the as prepared $\text{Mn}_2\text{Ru}_{0.5}\text{Co}_{0.5}\text{Sn}$ and $\text{Mn}_2\text{Ru}_{0.35}\text{Co}_{0.65}\text{Sn}$ ribbons with the corresponding experimental patterns. The peaks marked by * sign in figure (b) are from Mn_2Sn secondary phase.

TABLE I. Lattice parameter (a) and density of $\text{Mn}_2\text{Ru}_{0.5}\text{Co}_{0.5}\text{Sn}$ and $\text{Mn}_2\text{Ru}_{0.35}\text{Co}_{0.65}\text{Sn}$ alloys.

Samples	Lattice parameter a (Å) with vacuum annealing at		Density (g/cm ³) with vacuum annealing at	
	None	450 °C	None	450 °C
$\text{Mn}_2\text{Ru}_{0.5}\text{Co}_{0.5}\text{Sn}$	6.15	6.14	8.83	8.87
$\text{Mn}_2\text{Ru}_{0.35}\text{Co}_{0.65}\text{Sn}$	6.12	6.10	8.78	8.85

The simulated powder diffraction patterns and corresponding experimental patterns for the as prepared samples are shown in Fig. 1(c). The lattice parameters and densities of the alloys as obtained from the Rietveld analysis are shown in Table I. The grain sizes in the ribbons as determined from the Rietveld analysis of the XRD patterns for both the samples are about 70 nm indicating that the rapidly quenched ribbons consist of nanostructured materials.

The structural properties including crystal structure and grain size of these alloys are highly stable against vacuum annealing of up to 450 °C, although there is a noticeable decrease in the lattice parameter. The decrease in the lattice parameter is consistent with the fact that Co atoms with relatively smaller atomic sizes partially replace the Ru atoms in the Mn_2RuSn lattice. Further, there are a few unindexed peaks in the XRD patterns of the cobalt-rich samples, which have been identified as the reflections from Mn_2Sn impurity phase. The fraction of this phase from Rietveld analysis has been estimated to be ~ 7 wt. %.

B. Magnetic properties

The magnetizations as a function of magnetic field $M(H)$ measured at room temperature for $\text{Mn}_2\text{Ru}_{0.5}\text{Co}_{0.5}\text{Sn}$ and $\text{Mn}_2\text{Ru}_{0.35}\text{Co}_{0.65}\text{Sn}$ ribbons are shown in Figs. 2(a) and

2(b), respectively. The $M(H)$ loops are nearly saturated at 30 kOe and are similar to those of a ferri- or ferromagnetic materials. Both the samples (before and after vacuum annealing) show soft magnetic properties with coercivities being between 30 Oe and 70 Oe. The $M(H)$ loops expanded near $H = 0$ Oe are shown as the insets of Figs. 2(a) and 2(b). These results also indicate that the samples have a small magnetic anisotropy. The room temperature magnetizations at 30 kOe for the as prepared $\text{Mn}_2\text{Ru}_{0.5}\text{Co}_{0.5}\text{Sn}$ and $\text{Mn}_2\text{Ru}_{0.35}\text{Co}_{0.65}\text{Sn}$ alloys are, respectively, 25 emu/g and 32 emu/g, and those for the annealed samples are displayed in Table II. The high-field magnetization (measured at 70 kOe) of $\text{Mn}_2\text{Ru}_{0.5}\text{Co}_{0.5}\text{Sn}$ at 5 K is 43 emu/g ($2.37 \mu_B/\text{f.u.}$), which is much higher than the value of saturation magnetization ($1.68 \mu_B/\text{f.u.}$) reported for Mn_2RuSn . Our experimental value is very close to the value ($2.5 \mu_B/\text{f.u.}$) expected for $\text{Mn}_2\text{Ru}_{0.5}\text{Co}_{0.5}\text{Sn}$ from the Slater-Pauling rule. The sample with higher concentration of Co, $\text{Mn}_2\text{Ru}_{0.35}\text{Co}_{0.65}\text{Sn}$, has exhibited a higher value of magnetization as a result of the increased number of ferromagnetically interacting Co-Co pairs, which is consistent with our first-principles calculations (see Sec. IV C below). As we see in Table II, the magnetizations of both the samples show a very small change with vacuum annealing at temperatures up to 450 °C.

The temperature dependent magnetizations $M(T)$ of the $\text{Mn}_2\text{Ru}_{0.5}\text{Co}_{0.5}\text{Sn}$ and $\text{Mn}_2\text{Ru}_{0.35}\text{Co}_{0.65}\text{Sn}$ ribbons were measured at 1 kOe between 55 K and 700 K and are shown in Figs. 3(a) and 3(b), respectively. The $M(T)$ curves of both the samples are smooth with single magnetic transitions at their Curie temperatures (T_c) as expected for the single phase ferri- or ferromagnetic materials. The T_c of the $\text{Mn}_2\text{Ru}_{0.5}\text{Co}_{0.5}\text{Sn}$ and $\text{Mn}_2\text{Ru}_{0.35}\text{Co}_{0.65}\text{Sn}$ ribbons, as determined from the point where the extrapolated paramagnetic downturn in $M(T)$ meets with the $M = 0$ line, are 448 K and 506 K, respectively. These values of T_c are much larger than the value ($T_c = 272.1$ K) reported for bulk Mn_2RuSn .¹⁶

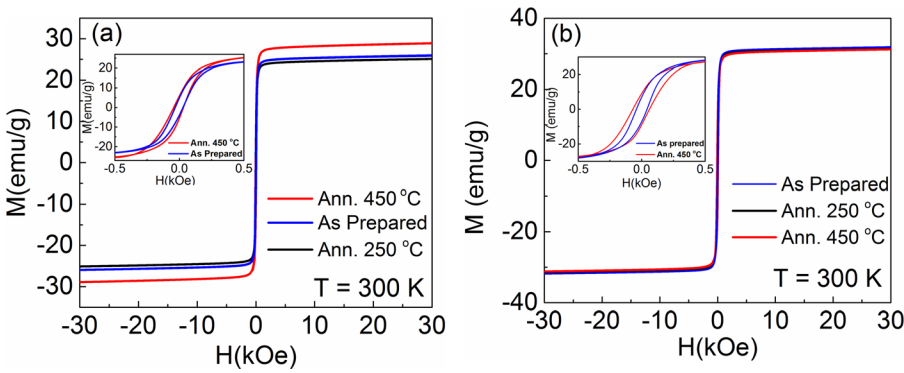


FIG. 2. The room-temperature magnetic field dependent magnetizations $M(H)$ of (a) $\text{Mn}_2\text{Ru}_{0.5}\text{Co}_{0.5}\text{Sn}$ and (b) $\text{Mn}_2\text{Ru}_{0.35}\text{Co}_{0.65}\text{Sn}$ ribbons. In both the figures, the insets show the portions of the $M(H)$ curves between -0.5 kOe and 0.5 kOe for the as-prepared and 450 °C-annealed samples.

TABLE II. Magnetizations and Curie temperatures of $\text{Mn}_2\text{Ru}_{0.5}\text{Co}_{0.5}\text{Sn}$ and $\text{Mn}_2\text{Ru}_{0.35}\text{Co}_{0.65}\text{Sn}$ alloys annealed at different temperatures.

Samples	T _c (K) with vacuum annealing at			M (emu/g) at 30 kOe with vacuum annealing at		
	None	250 °C	450 °C	None	250 °C	450 °C
$\text{Mn}_2\text{Ru}_{0.5}\text{Co}_{0.5}\text{Sn}$	448	438	435	25	26	29
$\text{Mn}_2\text{Ru}_{0.35}\text{Co}_{0.65}\text{Sn}$	506	501	490	32	31.5	31

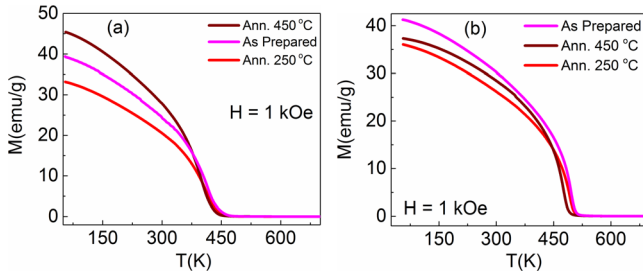


FIG. 3. The temperature dependent magnetizations $M(T)$ of (a) $\text{Mn}_2\text{Ru}_{0.5}\text{Co}_{0.5}\text{Sn}$ and (b) $\text{Mn}_2\text{Ru}_{0.35}\text{Co}_{0.65}\text{Sn}$ ribbons recorded at 1 kOe between 60 K and 700 K. In both the figures, $M(T)$ curves of as-prepared, 250 °C-annealed, and 450 °C-annealed samples are shown.

The huge increase in the Curie temperature of Mn_2RuSn as a fraction of Ru is replaced with Co indicates that the presence of Co in the Mn_2RuSn lattice significantly strengthens the positive exchange interaction suppressing the antiferromagnetic interaction. Both the samples show a small decrease in the Curie temperature due to vacuum annealing (see Table II). This may be caused by the thermal rearrangement of the magnetic atoms in the Mn_2RuSn lattice modifying the interaction among these atoms.

IV. FIRST-PRINCIPLES CALCULATIONS

A. Crystal structure

We have performed first-principles calculations with 16-atom cubic super-cell, $\text{Mn}_8\text{Ru}_4\text{Sn}_4$ in bulk geometry where the periodic boundary conditions are imposed. To simulate Co doping, we replace two Ru atoms with Co. We have considered two structures: (i) inverse Heusler (also called XA structure in Ref. 12), where 4 Mn and 4 Ru atoms occupy the 4a(0,0,0) and 4b(1/2,1/2,1/2) sites, respectively, while the other 4 Sn and the 4 Mn atoms enter, respectively, the 4c(1/4,1/4,1/4) and 4d(3/4,3/4,3/4) sites (see Fig. 4(a)); (ii) the $L_{2,B}$ structure,¹³ where Mn and Ru atoms occupy 4a and 4b sites randomly, as shown in Fig. 4(c). Figures 4(b) and 4(d) show corresponding structures with Co doping, i.e., $\text{Mn}_8\text{Ru}_2\text{Co}_2\text{Sn}_4$. Further, our calculations also show that Mn_2RuSn can undergo a phase transition to tetragonal structure consistent with the recent report,¹³ but in the present electronic and magnetic structure calculations we do not consider a tetragonal symmetry because our samples are cubic according to the XRD results.

We have calculated the equilibrium lattice parameters of Mn_2RuSn alloy for both the structures, with and without Co. Fig. 5 shows the energy versus lattice constant for XA structure. The behavior of the energy vs. lattice constant for the $L_{2,B}$ structure (not shown here) is identical (within the precision of our calculation) to that of the XA structure, which is also consistent with the previously reported results.^{13,14} This indicates

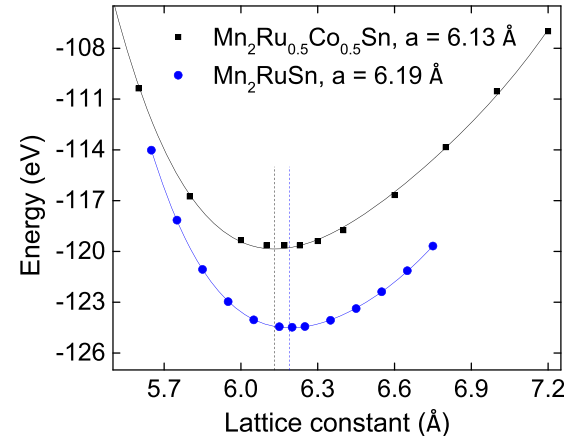
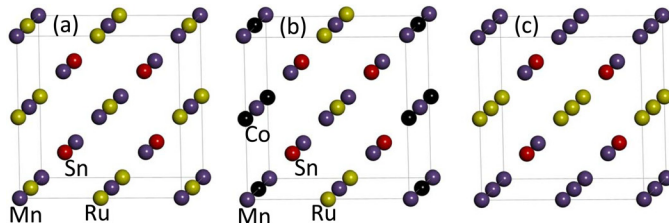


FIG. 5. Energy vs. lattice constant of $\text{Mn}_8\text{Ru}_4\text{Sn}_4$ (blue spheres) and $\text{Mn}_8\text{Ru}_2\text{Co}_2\text{Sn}_4$ (black squares). Vertical dashed lines point to the energy minimum.

that a certain degree of disorder between 4a and 4b sites is possible for the Mn and Ru atoms consistent with our Rietveld analysis of XRD patterns. As shown in Fig. 5, the equilibrium lattice constants are, respectively, $a = 6.19 \text{ \AA}$ for $\text{Mn}_8\text{Ru}_4\text{Sn}_4$ and $a = 6.13 \text{ \AA}$ for $\text{Mn}_8\text{Ru}_2\text{Co}_2\text{Sn}_4$, in good agreement with the values obtained from the Rietveld analysis of our experimental XRD data. This agreement between the experimental and calculated values of a is a clear indication that the substituted Co atoms have occupied the Ru sites in Mn_2RuSn lattice.

B. Electronic band structure

In order to investigate how the change in lattice constant caused by the substitution of Co for Ru modifies the ground state of Mn_2RuSn , we have calculated the electronic band structures of both $\text{Mn}_8\text{Ru}_4\text{Sn}_4$ and $\text{Mn}_8\text{Ru}_2\text{Co}_2\text{Sn}_4$ alloys. The densities of states (DOS) of $\text{Mn}_8\text{Ru}_4\text{Sn}_4$ and $\text{Mn}_8\text{Ru}_2\text{Co}_2\text{Sn}_4$ as a function of lattice constant for the XA and $L_{2,B}$ structures are shown in Figs. 6 and 7, respectively. First, we notice that reduction of the lattice constant results in the shift of the minority DOS leading to a half metallic state. For $\text{Mn}_8\text{Ru}_4\text{Sn}_4$, this transition occurs at approximately 6.10 \AA , i.e., close to the optimal lattice constant of $\text{Mn}_8\text{Ru}_2\text{Co}_2\text{Sn}_4$. Therefore, one could expect that the ground state of $\text{Mn}_8\text{Ru}_2\text{Co}_2\text{Sn}_4$ is either half metallic or very close to it. However, according to our results (Fig. 6(b), right panels), replacing 50% of Ru with Co in $\text{Mn}_8\text{Ru}_4\text{Sn}_4$ not only reduces the lattice constant, but also moves the transition to half metallicity to even lower lattice constant of about 6.0 \AA . Concerning the half metallicity, we have observed almost similar behavior for the $L_{2,B}$ structure as well (see Fig. 7).

As one can see from Figures 6 and 7, the dominant contribution to DOS at the optimal lattice constant around the

FIG. 4. 16-atom unit cells of $\text{Mn}_8\text{Ru}_4\text{Sn}_4$ and $\text{Mn}_8\text{Ru}_2\text{Co}_2\text{Sn}_4$ in XA (a) and (b), and in $L_{2,B}$ (c) and (d) phases. Atoms are color coded as follows: Mn—light blue, Ru—yellow, Sn—red, and Co—black.

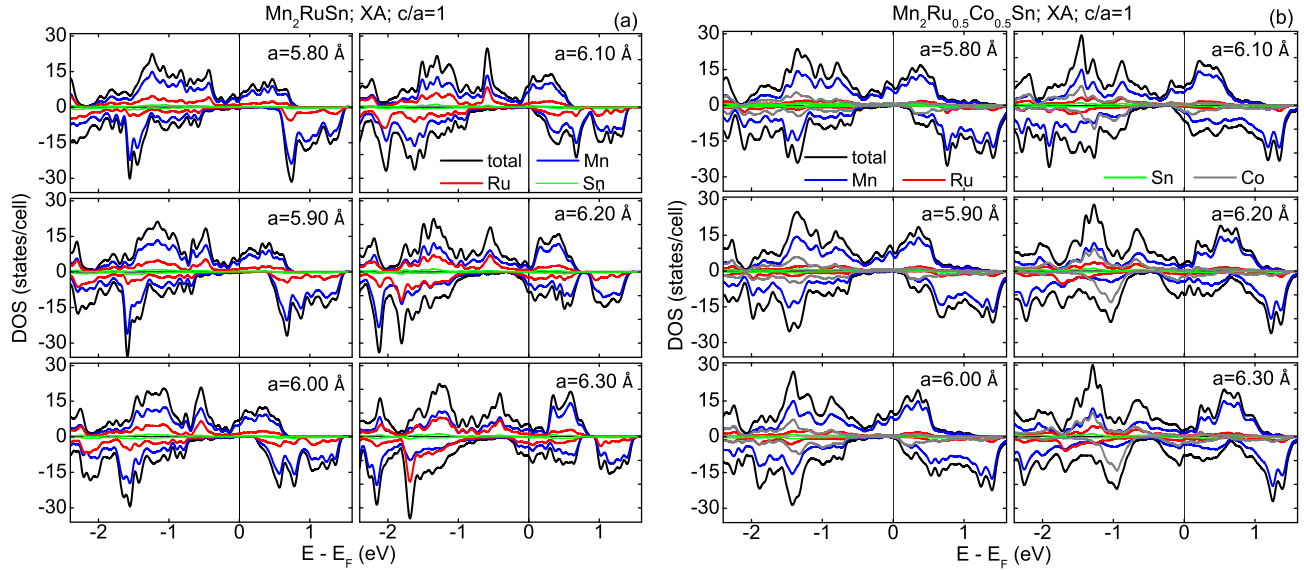


FIG. 6. DOS of $\text{Mn}_8\text{Ru}_4\text{Sn}_4$ (left panel—(a)) and $\text{Mn}_8\text{Ru}_2\text{Co}_2\text{Sn}_4$ (right panel—(b)), XA structure. Lattice constants are indicated on the plots. Vertical line corresponds to the Fermi level. Individual contributions to DOS are color coded, as indicated on the plot.

Fermi energy comes from the Mn states. This explains why the site disorder, i.e., transition from XA to $L2_1B$ structure, has only very minor effect on the behavior of half-metallicity as a function of lattice constant when fraction of Ru atoms is replaced with Co. Indeed, the half metallicity at smaller lattice constants results from the shift of the minority spin states to the energy values above the Fermi level, and this shift is not very sensitive to the replacement of Ru atoms with Co, since neither Ru nor Co have significant contribution to the minority spin DOS around Fermi level.

C. Magnetic structure

Our calculations show that the lowest energy states of $\text{Mn}_8\text{Ru}_4\text{Sn}_4$ and $\text{Mn}_8\text{Ru}_2\text{Co}_2\text{Sn}_4$ correspond to the ferrimagnetic spin structure, which agrees with the previous calculations

for $\text{Mn}_8\text{Ru}_4\text{Sn}_4$.¹³ The local magnetic moments per atom for both $\text{Mn}_8\text{Ru}_4\text{Sn}_4$ and $\text{Mn}_8\text{Ru}_2\text{Co}_2\text{Sn}_4$ calculated at their optimal lattice constants are presented in Table III. The calculated net magnetic moment of $1.5 \mu_B/\text{f.u.}$ for $\text{Mn}_8\text{Ru}_4\text{Sn}_4$ in XA structure is close to the experimentally reported value of 1.68 .¹⁶

At the same time, for $\text{Mn}_8\text{Ru}_4\text{Sn}_4$ in $L2_1B$ structure, the total net magnetic moment goes down to $1.1 \mu_B/\text{f.u.}$ $\text{Mn}_8\text{Ru}_2\text{Co}_2\text{Sn}_4$ in XA structure also has ferrimagnetic structure with the following moments: $-1.6 \mu_B$ and $-2.6 \mu_B$ on A sites (former corresponds to Mn atoms with 4 nearest neighbor Co, while the latter corresponds to Mn atoms with 2 nearest neighbor Co) and $3.3 \mu_B$ on B sites per Mn atom, $0.3 \mu_B$ per Ru, $0.03 \mu_B$ per Sn, and $1.0 \mu_B$ per Co (i.e., Co atoms indeed have ferromagnetic alignment). This results in $1.9 \mu_B/\text{f.u.}$ of total magnetic moment, which is close to our experimental saturation magnetization of $2.37 \mu_B/\text{f.u.}$ Interestingly, the total

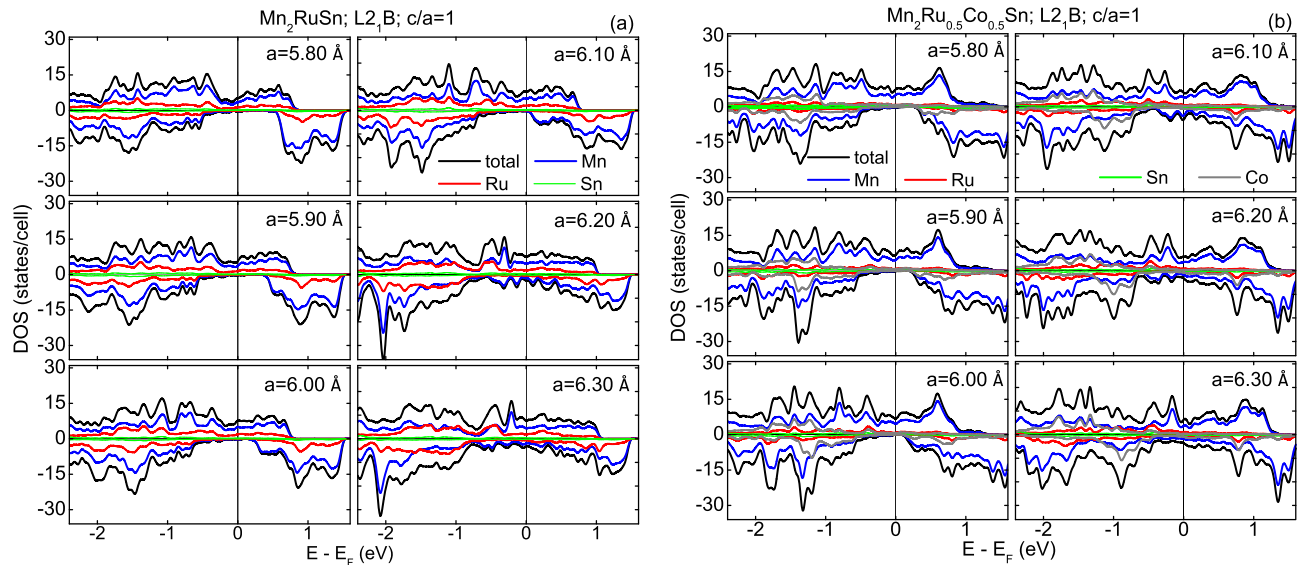


FIG. 7. DOS of $\text{Mn}_8\text{Ru}_4\text{Sn}_4$ (left panel—(a)) and $\text{Mn}_8\text{Ru}_2\text{Co}_2\text{Sn}_4$ (right panel—(b)), $L2_1B$ structure. Lattice constants are indicated on the plots. Vertical line corresponds to the Fermi level. Individual contributions to DOS are color coded, as indicated on the plot.

TABLE III. Atom resolved and total magnetic moments (in units of μ_B) for $Mn_8Ru_4Sn_4$ and $Mn_8Ru_2Co_2Sn_4$ in XA and $L2_1B$ structures. Mn-A and Mn-B correspond to the Mn atoms at A site and B sites, respectively.

	Mn-A	Mn-B	Ru	Sn	Co	Total ($\mu_B/f.u.$)
$Mn_8Ru_4Sn_4, XA$	-2.3	3.4	0.3	0.1	N/A	1.5
$Mn_8Ru_2Co_2Sn_4, XA$	-1.6; -2.5	3.3	0.3	0.03	1.0	1.9
$Mn_8Ru_4Sn_4, L2_1B$	-2.6	3.3	0.3	0.05	N/A	1.1
$Mn_8Ru_2Co_2Sn_4, L2_1B$	-2.2; -2.4	3.3	0.4	0.03	1.15	1.8

magnetic moment of $Mn_8Ru_2Co_2Sn_4$ in $L2_1B$ structure ($1.8 \mu_B/f.u.$) is very close to that in the XA structure indicating that the Co substituted samples are less sensitive to the structural disorder as compared to Mn_2RuSn . Thus, we see that replacing a fraction of Ru with Co results in significant suppression of the antiferromagnetic interaction, and favors positive exchange interactions without producing any noticeable change in the crystal structure. We also see that replacing larger fraction of Ru with Co should increase the total magnetic moment consistent with our experimental results.

V. CONCLUSIONS

The single phase $Mn_2Ru_{0.5}Co_{0.5}Sn$ and $Mn_2Ru_{0.35}Co_{0.65}Sn$ nanomaterials in cubic $L2_1B$ -type structure were synthesized using arc melting and melt spinning. The lattice parameters as determined by the Rietveld analysis are $a = 6.14 \text{ \AA}$, and 6.12 \AA for the as-prepared $Mn_2Ru_{0.5}Co_{0.5}Sn$ and $Mn_2Ru_{0.35}Co_{0.65}Sn$, respectively. The magnetic structure in these samples is ferri-magnetic with the Curie temperature being well above room temperature. There is a huge increase in the Curie temperature of Mn_2RuSn due to Co substitution, where the T_c for $Mn_2Ru_{0.5}Co_{0.5}Sn$ and $Mn_2Ru_{0.35}Co_{0.65}Sn$ are 448 K and 506 K, respectively. Both the materials are stable against heat treatment of up to 450 °C. Our first-principles calculations support the experimental findings. In particular, we confirm the experimental lattice parameters for Mn_2RuSn and $Mn_2Ru_{0.5}Co_{0.5}Sn$, as well as their ferri-magnetic alignment. We also show that replacing a fraction of Ru with Co significantly suppresses the antiferromagnetic interaction, thus favoring positive exchange interactions. Also, we find that the magnetic and electronic band properties of $Mn_2Ru_{0.5}Co_{0.5}Sn$ are less sensitive to disorder than those of Mn_2RuSn . These results are interesting scientifically and also suggest that $Mn_2Ru_{0.5}Co_{0.5}Sn$ may have potential for above-room-temperature technological applications.

ACKNOWLEDGMENTS

This research was supported by Academic and Scholarly Excellence Funds, Office of Academic Affairs, South Dakota State University. The research at the University of Nebraska was supported by NSF-MRSEC-DMR-4820521 (P.K., R.F.) and DOE-BES-Grant DE-FG02-04ER46152 (W.Z., D.J.S.). The research was performed in part in the Central Facilities of the Nebraska Center for Materials and Nanoscience, which is supported by the Nebraska Research Initiative. P.L. acknowledges financial support of the Pre-Tenure Grant from the Office of the Provost & Executive Vice President for Academic Affairs, University of Northern Iowa. Computations were performed at the University of Nebraska, Holland Computing Center and at the University of Northern Iowa, Department of Physics computing facilities.

- ¹B. Balke, G. H. Fecher, J. Winterlik, and C. Felser, *Appl. Phys. Lett.* **90**, 152504 (2007).
- ²H. Kurt, K. Rode, M. Venkatesan, P. Stamenov, and J. M. D. Coey, *Phys. Status Solidi B* **248**, 2338 (2011).
- ³R. A. de Groot, F. M. Mueller, P. G. van Engen, and K. H. J. Buschow, *Phys. Rev. Lett.* **50**, 2024 (1983).
- ⁴J. Winterlik, S. Chadov, A. Gupta, V. Aljani, T. Gasi, K. Filsinger, B. Balke, G. H. Fecher, C. A. Jenkins, F. Casper, J. Kübler, G. Liu, L. Gao, S. S. P. Parkin, and C. Felser, *Adv. Mater.* **24**, 6283 (2012).
- ⁵T. Krenke, E. Duman, M. Acet, E. F. Wassermann, X. Moya, L. Mañosa, and A. Planes, *Nature Mater.* **4**, 450 (2005).
- ⁶I. Takeuchi, O. O. Famodu, J. C. Read, M. A. Aronova, K.-S. Chang, C. Craciunescu, S. E. Lofland, M. Wuttig, F. C. Wellstood, L. Knauss, and A. Orozco, *Nature Mater.* **2**, 180 (2003).
- ⁷Y. Huh, P. Kharel, V. R. Shah, E. Krage, R. Skomski, J. E. Shield, and D. J. Sellmyer, *IEEE Trans. Magn.* **49**, 3277 (2013).
- ⁸S. Ouardi, G. H. Fecher, and C. Felser, *Phys. Rev. Lett.* **110**, 100401 (2013).
- ⁹X. L. Wang, *Phys. Rev. Lett.* **100**, 156404 (2008).
- ¹⁰M. E. Jamer, B. A. Assaf, T. Devakul, and D. Heiman, *Appl. Phys. Lett.* **103**, 142403 (2013).
- ¹¹T. Graf, C. Felser, and S. S. P. Parkin, *Prog. Solid State Chem.* **39**, 1–50 (2011).
- ¹²L. Yang, B. Liu, F. Meng, H. Liu, H. Luo, E. Liu, W. Wang, and G. Wu, *J. Magn. Magn. Mater.* **379**, 1 (2015).
- ¹³J. Chen, H. Luo, P. Jia, F. Meng, G. Liu, E. Liu, W. Wang, and G. Wu, *J. Magn. Magn. Mater.* **365**, 132 (2014).
- ¹⁴L. Yang, B. Liu, H. Luo, F. Meng, H. Liu, E. Liu, W. Wang, and G. Wu, *J. Magn. Magn. Mater.* **382**, 247 (2015).
- ¹⁵G. Kreiner, A. Kalache, S. Hausdorf, V. Aljani, J. F. Quian, G. Shan, U. Burkhardt, S. Ouardi, and C. Felser, *Z. Anorg. Allg. Chem.* **640**, 738 (2014).
- ¹⁶K. Endo, T. Kanomata, H. Nishihara, and K. R. A. Ziebeck, *J. Alloys Compd.* **510**, 1 (2012).
- ¹⁷TOPAS-V 4.2, Bruker AXS, Inc, 2009.
- ¹⁸P. Blöchl, *Phys. Rev. B* **50**, 17953 (1994).
- ¹⁹G. Kresse and D. Joubert, *Phys. Rev. B* **59**, 1758 (1999).
- ²⁰J. P. Perdew, K. Burke, and M. Ernzerhof, *Phys. Rev. Lett.* **77**, 3865 (1996).
- ²¹M. Methfessel and A. T. Paxton, *Phys. Rev. B* **40**, 3616 (1989).

Journal of Applied Physics is copyrighted by AIP Publishing LLC (AIP). Reuse of AIP content is subject to the terms at: <http://scitation.aip.org/termsconditions>. For more information, see <http://publishing.aip.org/authors/rights-and-permissions>.